Nonequilibrium Steady-State Transport in Quantum Impurity Models: A Thermofield and Quantum Quench Approach Using Matrix Product States

F. Schwarz,[1] I. Weymann,[2] J. von Delft,[1] and A. Weichselbaum[1,3,*]
[1]*Physics Department, Arnold Sommerfeld Center for Theoretical Physics, and Center for NanoScience, Ludwig-Maximilians-Universität, Theresienstraße 37, 80333 München, Germany*
[2]*Faculty of Physics, Adam Mickiewicz University, Umultowska 85, 61-614 Poznań, Poland*
[3]*Department of Condensed Matter Physics and Materials Science, Brookhaven National Laboratory, Upton, New York 11973-5000, USA*

(Received 28 August 2017; revised manuscript received 21 December 2017; published 26 September 2018)

The numerical renormalization group (NRG) is tailored to describe interacting impurity models in equilibrium, but it faces limitations for steady-state nonequilibrium, arising, e.g., due to an applied bias voltage. We show that these limitations can be overcome by describing the thermal leads using a thermofield approach, integrating out high energy modes using NRG, and then treating the nonequilibrium dynamics at low energies using a quench protocol, implemented using the time-dependent density matrix renormalization group. This yields quantitatively reliable results for the current (with errors $\lesssim 3\%$) down to the exponentially small energy scales characteristic of impurity models. We present results of benchmark quality for the temperature and magnetic field dependence of the zero-bias conductance peak for the single-impurity Anderson model.

DOI: 10.1103/PhysRevLett.121.137702

Introduction.—A major open problem in the theoretical study of nanostructures, such as quantum dots or nanowires, is the reliable computation of the nonlinear conductance under the conditions of nonequilibrium steady-state (NESS) transport. These are open quantum systems featuring strong local interactions, typically described by quantum impurity models such as the interacting resonant level model (IRLM), the Kondo model (KM), or the single-impurity Anderson model (SIAM). Much work has been devoted to studying the NESS properties of such models using a variety of methods [1–15], leading to a fairly good qualitative understanding of their behavior. The interplay of strong correlations, NESS driving, and dissipative effects leads to a rich and complex phenomenology. In particular, for the KM and SIAM, the nonlinear conductance exhibits a striking zero-bias peak, the so-called Kondo peak, characterized by a small energy scale, the Kondo temperature T_K, that weakens with increasing temperature and splits with increasing magnetic field, in qualitative agreement with experiments [16–22]. However, a full, quantitative description of the NESS behavior of such models under generic conditions has so far been unfeasible: none of the currently available approaches meet the three-fold challenge of (i) treating interactions essentially exactly, (ii) resolving very small energy scales, and (iii) incorporating NESS conditions.

This Letter presents an approach that does meet this challenge. (i) To deal with interactions, we use numerical matrix product state (MPS) methods. (ii) We use the numerical renormalization group (NRG) [23,24] to integrate out high-energy modes, leading to a renormalized impurity problem [25] whose reduced effective bandwidth, D^*, is set by a transport window defined by the voltage bias (V) and the temperature (T). This considerably enlarges the window of accessible time scales, which scale as $1/D^*$, and thus it enables us to treat arbitrary voltages. (iii) We then study the transport properties of the renormalized problem using a quench protocol where we abruptly switch on the impurity-lead coupling and compute the subsequent time evolution of the current, $J(t)$, using the time-dependent density-matrix renormalization group (TDMRG) [26–29]. Whereas similar

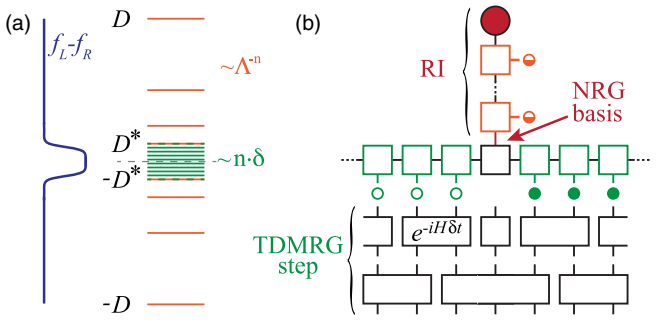

FIG. 1. (a) The discretization combines a log-sector for high energy excitations with a lin-sector for the TW. (b) The log-sector is treated using NRG. Here, "holes" and "particles" are recombined. The effective low-energy basis of NRG is used as the local state space of one MPS chain element. For the lin-sector, holes (empty at $t = 0$) and particles (filled at $t = 0$) are treated separately. On the chain including the RI, we do a TDMRG calculation based on a Trotter decomposition in "odd" and "even" bonds [37].

protocols [5,15,30,31] typically work at $T = 0$, we consider nonequilibrium thermal leads for arbitrary T, using the thermofield approach [32–36] to describe them with a pure product state in an enlarged Hilbert space.

We benchmark our approach using the IRLM, finding excellent agreement with exact Bethe-ansatz predictions for the NESS current. We then turn to the SIAM. For the linear conductance, we reproduce equilibrium NRG results. For the nonlinear conductance, we study the evolution of the zero-bias peak with T and magnetic field.

Setup.—We consider impurities coupled to two thermal leads, labeled $\alpha \in \{L, R\}$ and characterized by Fermi functions $f_\alpha(\omega) = (e^{(\omega-\mu_\alpha)/T}+1)^{-1}$, where $\mu_{L/R} = \pm V/2$. (We set $e = \hbar = k_B = 1$.) We study two different models, the spinless IRLM with a three-site impurity and Coulomb repulsion U between neighboring sites, and the SIAM with Coulomb repulsion U between different spins and a Zeeman splitting due to a magnetic field B. The impurities of these models are described by

$$H_{\mathrm{imp}}^{(\mathrm{I})} = \varepsilon_d \hat{n}_C + U(\hat{n}_L + \hat{n}_R - 1)\hat{n}_C + (t' d_C^\dagger d_L + t' d_C^\dagger d_R + \mathrm{H.c.}) \tag{1}$$

$$H_{\mathrm{imp}}^{(\mathrm{S})} = \varepsilon_d(\hat{n}_{d\uparrow} + \hat{n}_{d\downarrow}) + U\hat{n}_{d\uparrow}\hat{n}_{d\downarrow} - \frac{B}{2}(\hat{n}_{d\uparrow} - \hat{n}_{d\downarrow}), \tag{2}$$

where $\hat{n}_i = d_i^\dagger d_i$, for $i \in \{L, R, C, d\uparrow, d\downarrow\}$. In this Letter, we focus on the particle-hole symmetric case ($\varepsilon_d = 0$ for the IRLM and $\varepsilon_d = -(U/2)$ for the SIAM). The leads are assumed to be noninteracting,

$$H_{\mathrm{lead}}^{(\mathrm{I/S})} = \sum_{\alpha(\sigma)k} \varepsilon_k c_{\alpha(\sigma)k}^\dagger c_{\alpha(\sigma)k} \equiv \sum_q \varepsilon_q c_q^\dagger c_q, \tag{3}$$

with spin index $\sigma \in \{\uparrow, \downarrow\}$ for the SIAM, $q \equiv \{\alpha, (\sigma), k\}$ a composite index, and k a label for the energy levels. The impurity-leads hybridization is given by

$$H_{\mathrm{hyb}}^{(\mathrm{I/S})} = \sum_q (v_q d_{\alpha/\sigma}^\dagger c_q + \mathrm{H.c.}), \tag{4}$$

where in the IRLM the left (right) impurity site d_L (d_R) couples to the modes c_{Lk} (c_{Rk}), respectively, while in the SIAM the two spin states d_σ couple to the lead modes $c_{\alpha\sigma k}$ spin-independently, $v_q = v_{\alpha k}$. The couplings v_q induce an impurity-lead hybridization $\Gamma_\alpha(\omega) = \pi \sum_{k\sigma} |v_q|^2 \delta(\omega - \varepsilon_q)$, chosen such that they represent a box distribution $\Gamma_\alpha(\omega) = \Gamma_\alpha \Theta(D - |\omega|)$ in the continuum limit with half-bandwidth $D := 1$ set as the unit of energy, unless specified otherwise. For the IRLM, we set $\Gamma_L = \Gamma_R = 0.5D$ corresponding to the hopping element of a tight-binding chain with half-bandwidth D, and for the SIAM, we likewise choose $\Gamma_L = \Gamma_R$ and define the total hybridization $\Gamma = \Gamma_L + \Gamma_R$.

Strategy.—We describe the thermal leads decoupled from the impurity using the thermofield approach [32–35]. The impurity-lead coupling induces nonequilibrium processes, which occur on energy scales corresponding to the *transport window* (TW), defined as the energy range in which $f_L(\omega) \gtrapprox f_R(\omega)$. Energy scales far outside of this TW are effectively in equilibrium, and we therefore integrate them out using NRG, whereas we describe the nonequilibrium physics within the TW using TDMRG quench. We implement both the NRG and TDMRG using MPS techniques. We use a logarithmically discretized sector (log-sector), representing the energy range of the leads outside of the TW, and a linearly discretized sector (lin-sector) within the TW, as depicted in Fig. 1(a). The transition from the logarithmic to the linear discretization can be smoothed [37]. To simplify the MPS calculation, we map the leads onto a chain, with on-site and nearest-neighbor terms only, by tridiagonalizing the Hamiltonian. Integrating out the log-sector using NRG we get a *renormalized impurity* (RI) [25] and a reduced effective bandwidth, $2D^*$, of order of the size of the TW. This enables us to treat transport on energy scales much smaller than D. In particular, we can study arbitrary ratios of V/T_K in the SIAM, even if $T_K \ll D$. We then turn on the coupling between the log-sector and lin-sector by performing a TDMRG quench, starting from an initial state $|\Psi_{\mathrm{ini}}\rangle = |\phi_{\mathrm{ini}}\rangle \otimes |\Omega_{\mathrm{lin}}\rangle$, where $|\phi_{\mathrm{ini}}\rangle$ describes the initial state of the RI, and $|\Omega_{\mathrm{lin}}\rangle$ is a *pure product state* describing the lin-sector of the thermal leads in the thermofield approach. To describe steady-state properties, we time-evolve $|\Psi_{\mathrm{ini}}\rangle$ until expectation values are stationary up to oscillations around their mean value. Since the effective bandwidth relevant for this TDMRG calculation is given by D^*, not D, exponentially large time scales of order $1/D^* \gg 1/D$ are accessible.

Thermofield description of decoupled leads.—In the context of MPS methods, the thermofield description [32–35] of the decoupled leads has two advantages: finite temperature states are represented as pure states, and thermal leads are described by a simple product state.

Akin to purification [29], we double our Hilbert space by introducing one auxiliary mode c_{q2} (not coupled to the system) for each lead mode $c_{q1} = c_q$. In this enlarged Hilbert space, we define a pure state $|\Omega\rangle$ such that the thermal expectation value of an operator A acting on the original physical lead is given by $\langle A \rangle = \langle \Omega | A | \Omega \rangle$. This state can be written as [37]

$$|\Omega\rangle = \prod_q \underbrace{\left(\sqrt{1-f_q}\,|0,1\rangle_q + \sqrt{f_q}\,|1,0\rangle_q\right)}_{\equiv |\tilde{0},\tilde{1}\rangle_q}, \tag{5}$$

with $f_q = f_\alpha(\varepsilon_q)$, where $|0,1\rangle_q$ and $|1,0\rangle_q$ are defined by $c_{q1}|0,1\rangle_q = c_{q2}^\dagger |0,1\rangle_q = c_{q1}^\dagger |1,0\rangle_q = c_{q2}|1,0\rangle_q = 0$ for all q. We map $|\Omega\rangle$ to a pure product state using the rotation

$$\begin{pmatrix} \tilde{c}_{q1} \\ \tilde{c}_{q2} \end{pmatrix} = \begin{pmatrix} \sqrt{1-f_q} & -\sqrt{f_q} \\ \sqrt{f_q} & \sqrt{1-f_q} \end{pmatrix} \begin{pmatrix} c_{q1} \\ c_{q2} \end{pmatrix}. \quad (6)$$

Having $\tilde{c}_{q1}|\Omega\rangle = \tilde{c}^{\dagger}_{q2}|\Omega\rangle = 0$, the modes $\tilde{c}_{q1}$ ($\tilde{c}_{q2}$) can be interpreted as holes (particles) which are empty (filled) in the thermal state, respectively. Since in Eq. (5) we constructed $|\Omega\rangle$ to be an eigenstate of the particle number operator, it remains so in the rotated basis. The physical and auxiliary modes are decoupled in the unrotated basis; hence we are free to choose an arbitrary Hamiltonian (and hence time evolution) for the auxiliary modes [47]. We choose their single-particle energies equal to those of the physical modes, $\varepsilon_{q2} = \varepsilon_q$, in order to ensure that the resulting total lead Hamiltonian is diagonal in j in both the original *and* the rotated basis:

$$\mathcal{H}_{\text{lead}} \equiv H_{\text{lead}} + H_{\text{aux}} = \sum_{qj} \varepsilon_q c^{\dagger}_{qj} c_{qj} = \sum_{qj} \varepsilon_q \tilde{c}^{\dagger}_{qj} \tilde{c}_{qj}. \quad (7)$$

Equation (4) is rotated into $H^{(\text{I/S})}_{\text{hyb}} = \sum_{qj} (\tilde{v}_{qj} d^{\dagger}_{\alpha/\sigma} \tilde{c}_{qj} + \text{H.c.})$, whose couplings, $\tilde{v}_{q1} = v_q\sqrt{1-f_q}$ and $\tilde{v}_{q2} = v_q\sqrt{f_q}$, now *explicitly depend* on the Fermi function and encode all relevant information about temperature and voltage.

For the SIAM, we use a specific linear combination of $\tilde{c}_{Lk\sigma i}$ and $\tilde{c}_{Rk\sigma i}$ modes, $\tilde{C}_{k\sigma i} \propto \sum_{\alpha} \tilde{v}_{\alpha k\sigma i} \tilde{c}_{\alpha k\sigma i}$, because the modes orthogonal to these [37] decouple. Mixing left and right lead modes is possible despite the nonequilibrium situation, because the difference in chemical potentials is accounted for by the V-dependent couplings $\tilde{v}_q$. In the IRLM, this reduction of modes is not possible because left and right lead couple to different impurity sites.

NRG renormalization of the impurity.—As is standard for NRG, we map the leads (in the thermofield representation) from the original "star geometry" to a chain geometry. To ensure that $|\Omega\rangle$ remains a product state, we perform the corresponding unitary transformation for holes and particles independently. This results in a chain consisting of two channels $i \in \{1, 2\}$ for the SIAM, and four for the IRLM due to the additional lead index $\alpha \in \{L, R\}$. The first part of the chain corresponds to the log-sector, the later part to the lin-sector. The hoppings within the log-sector decay as Λ^{-n}, because for each lead level q within the log-sector of the original star geometry, either $\tilde{c}_{q1}$ or $\tilde{c}_{q2}$ decouples from the RI due to $f_q \in \{0, 1\}$. For NRG calculations, it is unfavorable to describe holes and particles in separate chains, because then particle-hole excitations involve opposite levels of different chains. For that reason, we recombine the holes and particles of the log-sector into one chain using a further tridiagonalization. In the IRLM, this is done for each lead α independently. After that, the log-sector resembles a standard Wilson chain with hoppings that scale as $\Lambda^{-n/2}$, reflecting the fact that the log-sector is effectively in equilibrium. A sketch of the different geometries can be found in Fig. S2 of Ref. [37].

Using NRG, we find an effective low-energy many-body basis for the log-sector, which we interpret as the local state space of a RI, and we treat it as one chain element of our MPS chain. Coupled to this RI, we have the lin-sector of the leads, represented as two separate chains for holes and particles, as shown in the upper part of Fig. 1(b).

TDMRG quench.—We choose the initial state for the quench as the product state $|\Psi_{\text{ini}}\rangle = |\phi_{\text{ini}}\rangle \otimes |\Omega_{\text{lin}}\rangle$. This implies that for the lin-sector, we start with the state in which all holes (particles) are empty (filled). As the initial state of the RI, $|\phi_{\text{ini}}\rangle$, we choose a ground state of the NRG basis (in principle, one can choose any of the low-energy basis states whose excitation energy is well within the TW). We then switch on the coupling between the RI and the leads, smoothly over a short time window. The system time-evolves under the Hamiltonian $\hat{H} = H_{\text{imp}} + H_{\text{hyb}} + H_{\text{lead}} + H_{\text{aux}}$, $|\Psi(t)\rangle = e^{-i\hat{H}t}|\Psi_{\text{ini}}\rangle$. We perform the time evolution using TDMRG based on a second order Trotter decomposition, as depicted in Fig. 1(b), with a Trotter time step of order $1/D^*$. (Technical details can be found in Sec. S-3.C of Ref. [37].) The fact that this initial lead state is entanglement-free is advantageous for reaching comparatively long times. We extract NESS information from $\langle A(t)\rangle = \langle\Psi(t)|A|\Psi(t)\rangle$ within a window of intermediate times, large enough for post-quench transients to no longer dominate, but well below the recurrence time, where finite-size effects set in. We compute the current through the impurity site (SIAM) or the central impurity site (IRLM), respectively, using $J = \frac{1}{2}(J_L - J_R)$, where J_L (J_R) is the current that flows into the site from the left (right), respectively [37]. We are able to track the time evolution up to times of order $1/D^*$. Since $D^* \sim \max(V, T)$, this suffices to describe particle transport for any choice of V or T. However, processes on much smaller energy scales cannot necessarily be resolved (see Sec. S-4.C of [37] for details).

Interacting resonant level model.—We benchmark our method for the IRLM, for which Ref. [15] computed the steady-state current at $T = 0$ both numerically, using DMRG quenches, and analytically, using the exact Bethe ansatz. A universal scaling of the current-voltage characteristics was found at the self-dual point of the model, with the corresponding energy scale T_B scaling as $(t')^{3/4}$. (These results were very recently confirmed by Ref. [48].) Figure 2 presents a comparison of our data with the analytical expression for the universal scaling curve given in [15], for the current as function of voltage at $T = 0$ at the self-dual point $U \approx D$ and $\varepsilon_d = 0$. The agreement is excellent for a large range of t' values. For each value of t', T_B was used as a fit parameter; the resulting T_B values, shown in the inset, agree nicely with the scaling predicted in [15]. Using the fitted values of T_B, all data points deviate by less than 2% from the Bethe results. Our use of NRG to renormalize

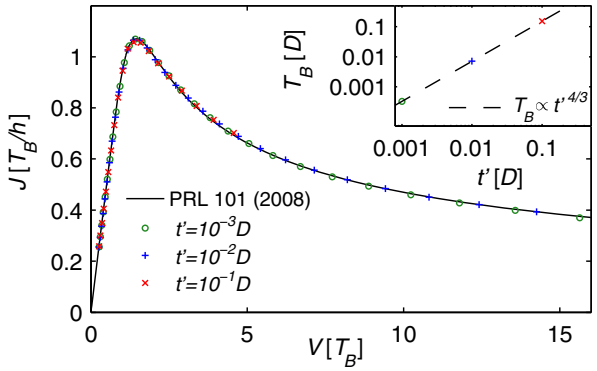

FIG. 2. Universal scaling of current vs voltage for the IRLM at the self-dual point for $T = 0$, in units of the energy scale $T_B(t')$, with negative differential conductance at large voltages, in excellent agreement with analytical results (solid curve, [15]). The inset shows the scaling of T_B with $(t')^{3/4}$.

the impurity enables us to study values of t' up to a hundred times smaller than the values used in [15], giving us access to much smaller values of T_B and larger V/T_B ratios.

Single-impurity Anderson model.—For the SIAM, a natural first check is the noninteracting case, $U = 0$, which is exactly solvable, but its treatment in MPS numerics does not differ from the case $U \neq 0$. The inset of Fig. 3(a) displays the current over voltage for two different temperatures, showing good agreement between our MPS numerics and exact predictions, thus providing direct evidence for the validity of our approach. For $U \neq 0$, our method yields quantitative agreement with previous numerical results obtained in the regime $V \gtrsim \Gamma$ [6,7], see Sec. S-6 of Ref. [37] for details. Furthermore, we find good agreement with the auxiliary master equation approach for arbitrary voltages, see Ref. [49] for details.

The main panel of Fig. 3(a) focuses on the differential conductance $g(T,V) = (\partial J(T,V)/\partial V)/(2e^2/h)$ for strong interactions. As a consistency check, we compare our results for $g(T,0)$ with the linear conductance computed using FDM-NRG [51]. We find excellent agreement over a large range of temperatures. From this data, we define the Kondo temperature T_K via the condition $g(T_K,0) \equiv \frac{1}{2}$.

We also show $g(0,V)$ over a wide voltage range in Fig. 3(a). In agreement with experiment [22] and other theoretical work [8], this curve lies above $g(T,0)$. The difference can be quantified by the value of $g(0,T_K)$, a universal number characterizing NESS transport for the SIAM, whose precise value is not yet known with quantitative certainty. Our method, which we trust to be quantitatively reliable, yields $g(0,T_K) \approx 0.60 \pm 0.02$ in the Kondo limit of $U/\Gamma \gg 1$, where the estimated error bar of about 3% is likely conservative (cf. [37]). For comparison, (nonexact) analytical calculations for the Kondo model yielded $g(0,T_K) \approx 2/3$ [8,9].

Figures 3(b)–3(d) show our quantitative description of the T- and B-dependence of the zero-bias peak in the Kondo limit ($U/\Gamma = 12$). With increasing T at $B = 0$, the zero-bias peak decreases [Fig. 3(b)], as observed in numerous experiments [17–22]. For finite B, the zero-bias peak splits into two sub-peaks at $V \approx \pm B$ [Fig. 3(c)]. A more detailed analysis of the value of B, at which the peak begins to split [52,53], is given in Sec. S-7 of Ref. [37]. In Fig. 3(d), the peak position with respect to B is resolved in more detail, with the voltage given in units of B. While for $B \approx 2T_K$ the peak position is roughly at $V/B \approx 0.83$, it quickly tends towards $V/B = 1$ for larger magnetic fields. Our study thus quantitatively confirms that the large-field peak-to-peak splitting for the nonlinear conductance is $\approx 2B$, as observed in several experiments [16,17,20]. This is also found in independent calculations [49] using the approach of Ref. [13].

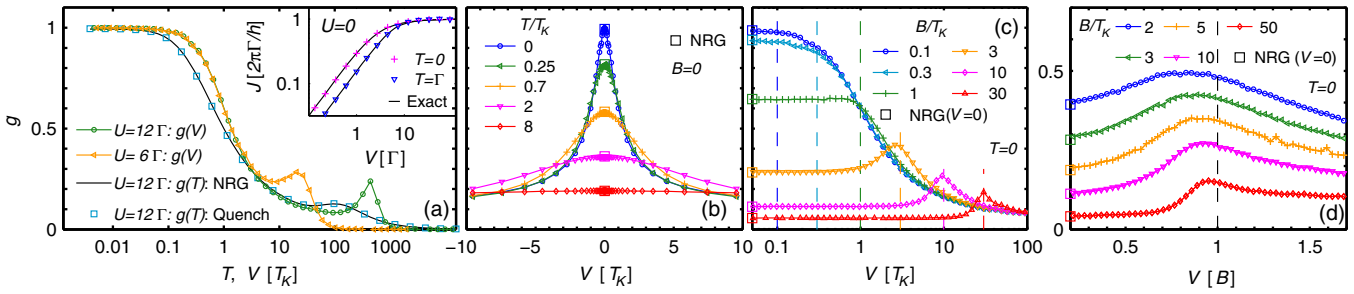

FIG. 3. Numerical results for the SIAM with $\Gamma = 10^{-3}$. For $U = 12\Gamma$, used in (b)–(d), we find $T_K = 2.61 \times 10^{-5}$. [This implies $T_K = 1.04 T_K^{(\chi)}$, where $T_K^{(\chi)} = (1/4\chi_s) = (U\Gamma/2)^{\frac{1}{2}} e^{\pi[(\Gamma/2U)-(U/8\Gamma)]}$ is an alternative definition of the Kondo temperature based on the Bethe-ansatz result [50] for the static spin susceptibility χ_s, at $B = T = 0$]. (a) Conductance vs V and T: squares show quench results in linear response as function of T, $g(T,0)$, in good agreement with the NRG results (solid line). Dots and triangles show quench results for the nonlinear conductance vs V at $T = 0$ for two different values of U. Inset: current vs V for $U = 0$ on a log-log scale, for two different temperatures, showing excellent agreement with analytical results. (b) Disappearance of the Kondo resonance in $g(T,V)$ with increasing T at $B = 0$, with $g(T,-V) = g(T,V)$, by symmetry. (c) Splitting of the resonance in $g(0,V)$ for finite B. Two subpeaks emerge at $V \approx \pm B$, as marked by the dashed lines. (d) Similar data as in (c) but plotted vs V/B and on a linear scale. For $B = 2T_K$, the peak position in the conductance $g(0,V)$ is still slightly below B, but for a higher magnetic field, the peak clearly moves towards $V/B \approx 1$. In (b)–(d), the squares indicate the NRG result for $V = 0$.

Summary and outlook.—We have combined the thermofield approach with a hybrid NRG-TDMRG quench strategy to reach a longstanding goal: a versatile, flexible, and *quantitatively reliable* method for studying quantum impurity models in steady-state nonequilibrium. Because of these features, our scheme has the potential of developing into the method of choice for such settings, in the same way as NRG is the method of choice for equilibrium impurity models. Indeed, various quantitative benchmark tests have confirmed the accuracy of our scheme, and it can easily be applied to other models and setups. For example, a generalization to a finite temperature difference between the left and right lead would be straightforward. It would also be interesting to use our setup for quantitative studies of the nonequilibrium two-channel Kondo physics measured in [54], or to study impurity models with superconducting leads, since the hybrid NRG-TDMRG approach is ideally suited for dealing with the bulk gap.

Methodologically, our setup can straightforwardly be extended to study NESS physics, without resorting to a quench strategy, by including Lindblad driving terms in the Liouville equation, which are *local* on the MPS chain [55]. Although the direct time-evolution of such Lindblad equations based on tensor networks seems feasible [56], one could try to avoid the real-time evolution altogether, and target the steady-state directly, by looking for the density matrix that fulfills $\dot{\rho} = 0$ [57,58].

We thank F. Heidrich-Meisner and P. Werner for providing the reference data in Fig. S6. We acknowledge useful discussions with E. Arrigoni, M.-C. Bañuls, B. Bruognolo, A. Dorda, D. Fugger, M. Goldstein, and H. Schöller. This work was supported by the German-Israeli-Foundation through I-1259-303.10 and by the DFG through the excellence cluster NIM. A. W. was also supported by DFG WE4819/1-1 and WE4819/2-1. I. W. was supported by National Science Centre in Poland through the Project No. DEC-2013/10/E/ST3/00213.

*andreas.weichselbaum@lmu.de

[1] A. Rosch, J. Paaske, J. Kroha, and P. Wölfle, Nonequilibrium Transport Through a Kondo Dot in a Magnetic Field: Perturbation Theory and Poor Man's Scaling, Phys. Rev. Lett. **90**, 076804 (2003).

[2] S. Kehrein, Scaling and Decoherence in the Nonequilibrium Kondo Model, Phys. Rev. Lett. **95**, 056602 (2005).

[3] F. B. Anders, Steady-State Currents Through Nanodevices: A Scattering-States Numerical Renormalization-Group Approach to Open Quantum Systems, Phys. Rev. Lett. **101**, 066804 (2008).

[4] S. Kirino, T. Fujii, J. Zhao, and K. Ueda, Time-dependent DMRG study on quantum dot under a finite bias voltage, J. Phys. Soc. Jpn. **77**, 084704 (2008).

[5] F. Heidrich-Meisner, A. E. Feiguin, and E. Dagotto, Real-time simulations of nonequilibrium transport in the single-impurity Anderson model, Phys. Rev. B **79**, 235336 (2009).

[6] J. Eckel, F. Heidrich-Meisner, S. G. Jakobs, M. Thorwart, M. Pletyukhov, and R. Egger, Comparative study of theoretical methods for non-equilibrium quantum transport, New J. Phys. **12**, 043042 (2010).

[7] P. Werner, T. Oka, M. Eckstein, and A. J. Millis, Weak-coupling quantum Monte Carlo calculations on the Keldysh contour: Theory and application to the current-voltage characteristics of the Anderson model, Phys. Rev. B **81**, 035108 (2010).

[8] M. Pletyukhov and H. Schoeller, Nonequilibrium Kondo Model: Crossover from Weak to Strong Coupling, Phys. Rev. Lett. **108**, 260601 (2012).

[9] S. Smirnov and M. Grifoni, Keldysh effective action theory for universal physics in spin-$\frac{1}{2}$ Kondo dots, Phys. Rev. B **87**, 121302 (2013).

[10] G. Cohen, E. Gull, D. R. Reichman, and A. J. Millis, Green's Functions from Real-Time Bold-Line Monte Carlo Calculations: Spectral Properties of the Nonequilibrium Anderson Impurity Model, Phys. Rev. Lett. **112**, 146802 (2014).

[11] A. E. Antipov, Q. Dong, and E. Gull, Voltage Quench Dynamics of a Kondo System, Phys. Rev. Lett. **116**, 036801 (2016).

[12] F. Reininghaus, M. Pletyukhov, and H. Schoeller, Kondo model in nonequilibrium: Interplay between voltage, temperature, and crossover from weak to strong coupling, Phys. Rev. B **90**, 085121 (2014).

[13] A. Dorda, M. Ganahl, H. G. Evertz, W. von der Linden, and E. Arrigoni, Auxiliary master equation approach within matrix product states: Spectral properties of the nonequilibrium Anderson impurity model, Phys. Rev. B **92**, 125145 (2015).

[14] S. G. Jakobs, V. Meden, and H. Schoeller, Nonequilibrium Functional Renormalization Group for Interacting Quantum Systems, Phys. Rev. Lett. **99**, 150603 (2007).

[15] E. Boulat, H. Saleur, and P. Schmitteckert, Twofold Advance in the Theoretical Understanding of far-from-Equilibrium Properties of Interacting Nanostructures, Phys. Rev. Lett. **101**, 140601 (2008).

[16] D. C. Ralph and R. A. Buhrman, Kondo-Assisted and Resonant Tunneling via a Single Charge Trap: A Realization of the Anderson Model Out of Equilibrium, Phys. Rev. Lett. **72**, 3401 (1994).

[17] D. Goldhaber-Gordon, H. Shtrikman, D. Mahalu, D. Abusch-Magder, U. Meirav, and M. A. Kastner, Kondo effect in a single-electron transistor, Nature (London) **391**, 156 (1998).

[18] S. M. Cronenwett, T. H. Oosterkamp, and L. P. Kouwenhoven, A tunable Kondo effect in quantum dots, Science **281**, 540 (1998).

[19] F. Simmel, R. H. Blick, J. P. Kotthaus, W. Wegscheider, and M. Bichler, Anomalous Kondo Effect in a Quantum Dot at Nonzero Bias, Phys. Rev. Lett. **83**, 804 (1999).

[20] W. G. van der Wiel, S. D. Franceschi, T. Fujisawa, J. M. Elzerman, S. Tarucha, and L. P. Kouwenhoven, The Kondo effect in the unitary limit, Science **289**, 2105 (2000).

[21] A. V. Kretinin, H. Shtrikman, D. Goldhaber-Gordon, M. Hanl, A. Weichselbaum, J. von Delft, T. Costi, and D. Mahalu, Spin-$\frac{1}{2}$ Kondo effect in an InAs nanowire quantum dot: Unitary limit, conductance scaling, and Zeeman splitting, Phys. Rev. B **84**, 245316 (2011).

[22] A. V. Kretinin, H. Shtrikman, and D. Mahalu, Universal line shape of the Kondo zero-bias anomaly in a quantum dot, Phys. Rev. B **85**, 201301 (2012).
[23] K. G. Wilson, The renormalization group: Critical phenomena and the Kondo problem, Rev. Mod. Phys. **47**, 773 (1975).
[24] R. Bulla, T. A. Costi, and T. Pruschke, Numerical renormalization group method for quantum impurity systems, Rev. Mod. Phys. **80**, 395 (2008).
[25] F. Güttge, F. B. Anders, U. Schollwöck, E. Eidelstein, and A. Schiller, Hybrid NRG-DMRG approach to real-time dynamics of quantum impurity systems, Phys. Rev. B **87**, 115115 (2013).
[26] G. Vidal, Efficient Simulation of One-Dimensional Quantum Many-Body Systems, Phys. Rev. Lett. **93**, 040502 (2004).
[27] A. J. Daley, C. Kollath, U. Schollwöck, and G. Vidal, Time-dependent density-matrix renormalization-group using adaptive effective Hilbert spaces, J. Stat. Mech. (2004) P04005.
[28] S. R. White and A. E. Feiguin, Real-Time Evolution Using the Density Matrix Renormalization Group, Phys. Rev. Lett. **93**, 076401 (2004).
[29] U. Schollwöck, The density-matrix renormalization group in the age of matrix product states, Ann. Phys. (Amsterdam) **326**, 96 (2011).
[30] A. Branschädel, G. Schneider, and P. Schmitteckert, Conductance of inhomogeneous systems: Real-time dynamics, Ann. Phys. (Amsterdam) **522**, 657 (2010).
[31] L. G. G. V. D. da Silva, F. Heidrich-Meisner, A. E. Feiguin, C. A. Büsser, G. B. Martins, E. V. Anda, and E. Dagotto, Transport properties and Kondo correlations in nanostructures: Time-dependent DMRG method applied to quantum dots coupled to Wilson chains, Phys. Rev. B **78**, 195317 (2008).
[32] Y. Takahashi and H. Umezawa, Thermo field dynamics, Collective Phenomena **2**, 55 (1975).
[33] S. M. Barnett and B. J. Dalton, Liouville space description of thermofields and their generalisations, J. Phys. A **20**, 411 (1987).
[34] A. Das, Topics in finite temperature field theory," in *Quantum Field Theory—A 20th Century Profile*, edited by A. N. Mitra (Hindustan Book Agency, New Delhi, 2000) pp. 383–411.
[35] I. de Vega and M.-C. Bañuls, Thermofield-based chain-mapping approach for open quantum systems, Phys. Rev. A **92**, 052116 (2015).
[36] C. Guo, I. de Vega, U. Schollwöck, and D. Poletti, Stable-unstable transition for a Bose-Hubbard chain coupled to an environment, Phys. Rev. A **97**, 053610 (2018),
[37] See Supplemental Material at http://link.aps.org/supplemental/10.1103/PhysRevLett.121.137702, which includes Refs. [38–46], for details.
[38] V. L. Campo and L. N. Oliveira, Alternative discretization in the numerical renormalization-group method, Phys. Rev. B **72**, 104432 (2005).
[39] R. Žitko, Adaptive logarithmic discretization for numerical renormalization group methods, Comput. Phys. Commun. **180**, 1271 (2009).
[40] A. Weichselbaum, Discarded weight and entanglement spectra in the numerical renormalization group, Phys. Rev. B **84**, 125130 (2011); Tensor networks and the numerical renormalization group, Phys. Rev. B **86**, 245124 (2012); Non-Abelian symmetries in tensor networks: A quantum symmetry space approach, Ann. Phys. (Amsterdam) **327**, 2972 (2012).
[41] P. Corboz, R. Orús, B. Bauer, and G. Vidal, Simulation of strongly correlated fermions in two spatial dimensions with fermionic projected entangled-pair states, Phys. Rev. B **81**, 165104 (2010).
[42] G. Schneider and P. Schmitteckert, Conductance in strongly correlated 1D systems: Real-time dynamics in DMRG, arXiv:cond-mat/0601389.
[43] P. Wang and S. Kehrein, Flow equation calculation of transient and steady-state currents in the Anderson impurity model, Phys. Rev. B **82**, 125124 (2010).
[44] T. Barthel, U. Schollwöck, and S. R. White, Spectral functions in one-dimensional quantum systems at finite temperature using the density matrix renormalization group, Phys. Rev. B **79**, 245101 (2009).
[45] P. Schmitteckert, Calculating Green functions from finite systems, J. Phys. Conf. Ser. **220**, 012022 (2010).
[46] M. Hanl and A. Weichselbaum, Local susceptibility and Kondo scaling in the presence of finite bandwidth, Phys. Rev. B **89**, 075130 (2014).
[47] C. Karrasch, J. H. Bardarson, and J. E. Moore, Finite-temperature dynamical density matrix renormalization group and the Drude weight of spin-1/2 chains, Phys. Rev. Lett. **108**, 227206 (2012).
[48] K. Bidzhiev and G. Misguich, Out-of-equilibrium dynamics in a quantum impurity model: Numerics for particle transport and entanglement entropy, Phys. Rev. B **96**, 195117 (2017).
[49] D. M. Fugger, A. Dorda, F. Schwarz, J. von Delft, and E. Arrigoni, Nonequilibrium Kondo effect in a magnetic field: auxiliary master equation approach, New J. Phys. **20**, 013030 (2018).
[50] P. B. Wiegmann and A. M. Tsvelick, Exact solution of the Anderson model: I, J. Phys. C **16**, 2281 (1983); A. M. Tsvelick and P. B. Wiegmann, Exact solution of the Anderson model. II. Thermodynamic properties at finite temperatures, J. Phys. C **16**, 2321 (1983).
[51] A. Weichselbaum and J. von Delft, Sum-Rule Conserving Spectral Functions from the Numerical Renormalization Group, Phys. Rev. Lett. **99**, 076402 (2007).
[52] M. Filippone, C. P. Moca, A. Weichselbaum, J. von Delft, and C. Mora, At which magnetic field, exactly, does the Kondo resonance begin to split? a Fermi liquid description of the low-energy properties of the Anderson model, Phys. Rev. B **98**, 075404 (2018).
[53] A. Oguri and A. C. Hewson, Higher-Order Fermi-Liquid Corrections for an Anderson Impurity Away from Half Filling, Phys. Rev. Lett. **120**, 126802 (2018); Higher-order Fermi-liquid corrections for an Anderson impurity away from half filling: Equilibrium properties, Phys. Rev. B **97**, 045406 (2018); Higher-order Fermi-liquid corrections for an Anderson impurity away from half filling: Nonequilibrium transport, Phys. Rev. B **97**, 035435 (2018).
[54] Z. Iftikhar, S. Jezouin, A. Anthore, U. Gennser, F. D. Parmentier, A. Cavanna, and F. Pierre, Two-channel Kondo

effect and renormalization flow with macroscopic quantum charge states, Nature (London) **526**, 233 (2015).

[55] F. Schwarz, M. Goldstein, A. Dorda, E. Arrigoni, A. Weichselbaum, and J. von Delft, Lindblad-driven discretized leads for nonequilibrium steady-state transport in quantum impurity models: Recovering the continuum limit, Phys. Rev. B **94**, 155142 (2016).

[56] A. H. Werner, D. Jaschke, P. Silvi, M. Kliesch, T. Calarco, J. Eisert, and S. Montangero, Positive Tensor Network Approach for Simulating Open Quantum Many-Body Systems, Phys. Rev. Lett. **116**, 237201 (2016).

[57] J. Cui, J. I. Cirac, and M. C. Bañuls, Variational Matrix Product Operators for the Steady State of Dissipative Quantum Systems, Phys. Rev. Lett. **114**, 220601 (2015).

[58] E. Mascarenhas, H. Flayac, and V. Savona, Matrix-product-operator approach to the nonequilibrium steady state of driven-dissipative quantum arrays, Phys. Rev. A **92**, 022116 (2015).